# Numerical Simulation of the Flow, Temperature, and Concentration Fields in a Radio Frequency Plasma CVD Reactor

ZHAO GUO-YING AND ZHU CHING-WEN

*Abstract*—**A mathematical model is presented for the numerical simulation of the flow in a radio frequency (RF) plasma chemical, vapor, and deposition (CVD) reactor. The main parts include a plasma torch (2.5 cm in radius, 22.5 cm long), a reactor (2.5 cm in radius, 20.0 cm long), and a powder collector (4.0 cm in radius, 20 cm long) with a water-cooling tank at the center. The model is based on the solution of two-dimensional continuity, momentum, energy, and species equations in cylindrical coordinates simultaneously with the one-dimensional magnetic and electric-field equations. Detailed knowledge about the velocity, species distributions, and temperature field (both in the flow and in the wall which confines the flow) is obtained by the numerical method SIMPLER of Patankar and Spalding. The effect of some important parameters such as side injection slit width and swirl velocity are investigated. Calculation is made under atmospheric pressure at a power level of 8.4 kW with argon as a heating gas and $SiCl_4$, $NH_3$, $H_2$ as reactants. Owing to the lack of related reaction rate, the chemical reaction and crystallization are not taken into account. Some comments on the flow field in the reactor are made.**

## NOMENCLATURE

| | |
|---|---|
| $C_i$ | Mass concentration. |
| $C_p$ | Specific heat at constant pressure. |
| $D$ | Molecular diffusion coefficient. |
| $h$ | Side injection slit width. |
| $L_1$ | Length of the torch. |
| $L_t$ | Total length of the plasma CVD reaction chamber. |
| $M$ | Molecular weight of the mixture. |
| $M_i$ | Molecular weight of $i$ species. |
| $n$ | Unit exterior normals to the wall. |
| $p$ | Pressure. |
| $P$ | Local dissipation power. |
| $Q$ | Volume flow rate. |
| $Q_r$ | Fraction of the power lost by radiation. |
| $r$ | Radial coordinate. |
| $R_{in}$, $R_{out}$ | Radius of tangential inlet tubes. |
| $R_{st}$ | Radius of reaction chamber and collection chamber. |
| $R_0$ | Radius of the quartz tube. |
| $R_{ci}$ | Radius of the coil. |
| $R$ | Universal constant of gases. |
| $S_\phi$ | Source term. |
| $T$ | Temperature. |
| $u$ | Velocity in $x$ direction. |
| $v$ | Velocity in $r$ direction. |
| $w$ | Velocity in $\theta$ direction. |
| $x$ | Axial coordinate. |
| $\rho$ | Density. |
| $\mu$ | Viscosity. |
| $\phi$ | General dependent variable. |
| $\Gamma_\phi$ | Diffusion coefficient. |

Manuscript received December 23, 1985; revised March 11, 1986.

The authors are with the Institute of Mechanics, Chinese Academy of Sciences, Beijing, China.

IEEE Log Number 8609596.

## I. INTRODUCTION

CERAMIC WILL BECOME a most promising high-tech material in the near future, and the synthesis of ceramic material such as $Si_3N_4$ and SiC ultrafine powder is one of the new research subjects of great interest. Radio frequency (RF) plasma chemical, vapor, and deposition (CVD) method is one of the most ideal ones for the synthesis of ultrafine powder [11] and its equipment is schematically shown in Fig. 1 [1]. If we want to synthesize $Si_3N_4$ powder, we can use $SiCl_4$ and $NH_3$ as reactants. The main parts of the equipment include a plasma torch, a reactor, and a powder collector. The plasma torch (2.5 cm in radius, 22.5 cm long) consists of two concentric quartz tubes (radii 2.0 and 2.5 cm, respectively), and a working induction coil (3 turn), the first turn of which is just 1 cm under the end of the inner quartz tube. Argon is added into the inner tube as a heating gas, while $SiCl_4$ vapor is added into the outer tube along with argon as a carrier gas. An electromagnetic field will be induced when RF electric current is passing through the coil and plasma is maintained in the torch by ohmic heating. The reactor consists of an injection ring slit of 0.1-mm width for the injection of reactants such as $NH_3$ and $H_2$, and a reaction chamber, which is made of a high-quality graphite tube. The main part of the powder collector is a collection tube (4.0 cm in radius, 20 cm long) with a concentric water-cooled quenching tank (2.5 cm in radius) inserted into it. The reaction zone length and quenching rate can be regulated with the change of the amount of cooling water and the quenching tank length.

In order to increase the reaction rate and efficiency of CVD synthesis, we have made a numerical simulation to study how to enlarge the equipment to industrial scale. Boulos [3], [4] and Yoshida [5] made computations on the

0093-3813/86/0800-0531$01.00 © 1986 IEEE

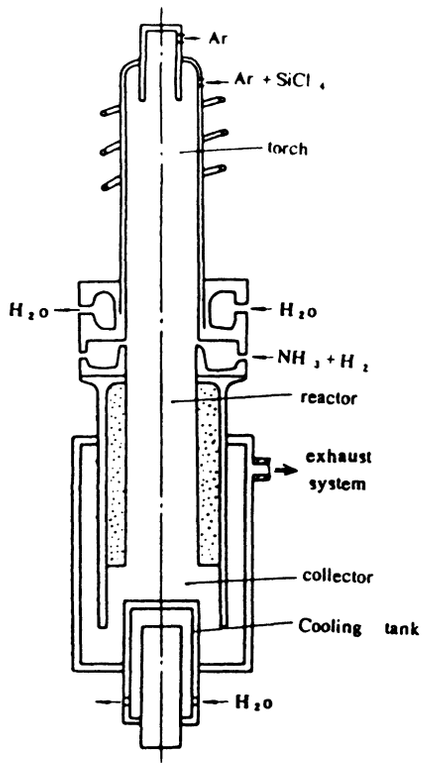


Fig. 1. Schematic representation of a plasma CVD reactor.

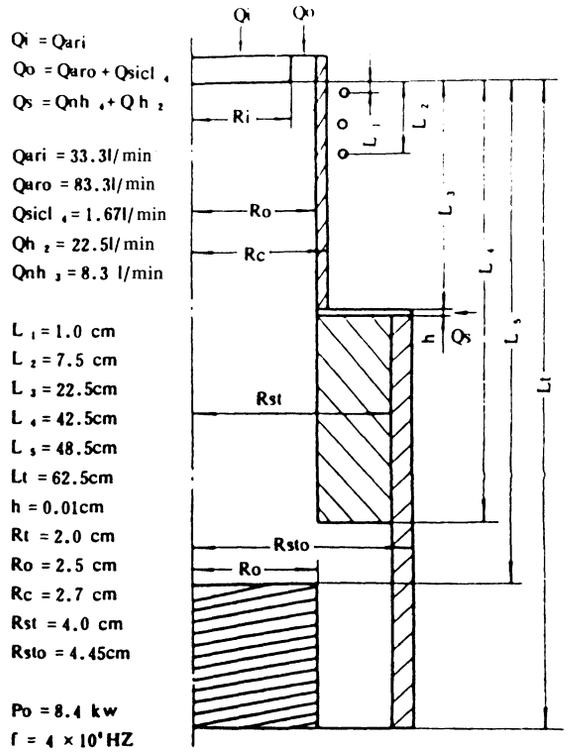


Fig. 2. Plasma CVD reactor geometry and its main operating conditions.

flow field in a plasma torch, while others [6] performed numerical simulation of the flow in a reactor under some simplification. Our simulation is made for the whole flow field including the torch and reactor under the operating condition. Because the flow involves electromagnetic heating, swirling, diffusion, chemical reaction, crystallization, and deposition, and the flow path is rather complex, it is valuable to study it using a numerical simulation. Having presented the result without heating in [2], we now present the result under atmospheric pressure at a power level of 8.4 kW with argon as the heating gas and $SiCl_4$, $NH_3$, and $H_2$ as reactants. Owing to the lack of related reaction rates, the chemical reaction and crystallization are not taken into account. Some comments on the flow field in the reactor are made.

## II. Governing Equations and Boundary Conditions

Fig. 1 schematically shows the plasma CVD reactor studied. Fig. 2 shows its configuration and main operating conditions.

The basic assumptions used are as follows:

1) two-dimensional flow and temperature fields and one-dimensional electric and magnetic fields;
2) there are no chemical reactions among species, and each species can be treated as a perfect gas;
3) local thermodynamic equilibrium;
4) steady-state laminar flow;
5) negligible viscous dissipation;
6) optically thin plasma; and
7) negligible displacement current.

Using cylindrical coordinates, the governing equations used can be formulated as follows.

Continuity:

$$\frac{\partial}{\partial x}(r\rho u) + \frac{\partial}{\partial r}(r\rho v) = 0. \tag{1}$$

Momentum ($\mu$ div $\bar{v} = 0$):

$$\frac{1}{r}\left[\frac{\partial}{\partial x}(r\rho u^2) + \frac{\partial}{\partial r}(r\rho uv)\right] = -\frac{\partial p}{\partial x} + \frac{1}{r}\left\{\frac{\partial}{\partial r}\left[r\mu\left(\frac{\partial u}{\partial r} + \frac{\partial v}{\partial x}\right)\right] + r\frac{\partial}{\partial x}\left(2\mu\frac{\partial u}{\partial x}\right)\right\} + \rho g \tag{2}$$

$$\frac{1}{r}\left[\frac{\partial}{\partial x}(r\rho uv) + \frac{\partial}{\partial r}(r\rho v^2) - \rho w^2\right] = -\frac{\partial p}{\partial r} + \left\{\frac{1}{r}\frac{\partial}{\partial r}\left(2\mu r\frac{\partial v}{\partial r}\right) - \frac{2\mu v}{r^2} + \frac{\partial}{\partial x}\left[\mu\left(\frac{\partial u}{\partial r} + \frac{\partial v}{\partial x}\right)\right]\right\} + F_r \tag{3}$$

$$\frac{1}{r}\left\{\left[\frac{\partial}{\partial x}(r\rho uw) + \frac{\partial}{\partial r}(r\rho vw)\right] + \rho vw\right\} = \frac{1}{r}\frac{\partial}{\partial r}\left[r^2\mu\frac{\partial}{\partial r}\left(\frac{w}{r}\right)\right] + \mu\frac{\partial}{\partial r}\left(\frac{w}{r}\right) + \frac{\partial}{\partial x}\left(\mu\frac{\partial w}{\partial x}\right). \tag{4}$$

Energy (neglect pressure work and dissipation):

$$\frac{1}{r}\overline{C}_p\left[\frac{\partial}{\partial x}(r\rho uT)+\frac{\partial}{\partial r}(r\rho vT)\right]=\frac{1}{r}\left[\frac{\partial}{\partial x}\left(rk\frac{\partial T}{\partial x}\right)+\frac{\partial}{\partial r}\left(rk\frac{\partial T}{\partial r}\right)\right]+\Sigma C_{pi}\left(\rho D_i\frac{\partial C_i}{\partial x}\right)\frac{\partial T}{\partial x}+\Sigma C_{pi}\rho D_i\left(\frac{\partial C_i}{\partial r}\right)\frac{\partial T}{\partial r}+(p-Q_r). \quad (5)$$

Diffusion (neglect the diffusion caused by the gradient of temperature):

$$\rho u\frac{\partial C_i}{\partial x}+\rho v\frac{\partial C_i}{\partial r}=\frac{1}{r}\left[\frac{\partial}{\partial x}\left(\rho D_i r\frac{\partial C_i}{\partial x}\right)+\frac{\partial}{\partial r}\left(\rho D_i r\frac{\partial C_i}{\partial r}\right)\right]. \quad (6)$$

Thermodynamic relations:

$$p=\rho RT/M$$
$$\overline{C}_p=\Sigma C_i C_{pi}$$
$$M=(\Sigma C_i/M_i)^{-1}. \quad (7)$$

Electromagnetic force and heating are obtained from the following Maxwell equations [4]:

$$\frac{dE_\theta}{dr}=-\frac{E_\theta}{r}-\xi\omega H_x\sin x \quad (8)$$

$$\frac{dH_x}{dT}=-\sigma E_\theta\cos x \quad (9)$$

$$\frac{dx}{dr}=\frac{\sigma E_\theta}{H_x}\sin x-\frac{\xi\omega H_x}{E_\theta}\cos x$$
$$p=\sigma E_\theta^2$$
$$F_r=\xi\sigma E_\theta H_x\cos x. \quad (10)$$

Since the plasma exists just in the center of the torch and the amount of $SiCl_4$ from the outer inlet is much less than that of argon, from the whole inlet we can assume the electromagnetic heating region is full of argon, so [4]

$$\sigma=\begin{cases}2.26\times10^4\exp(-6.21\times10^4/T)\ 1/\text{cm}\cdot\Omega, & T\le 8000\ \text{K}\\ 1.96\times10^4\exp(-4.26\times10^4/T)\ 1/\text{cm}\cdot\Omega, & 8000\ \text{K}<T<15\,000\ \text{K}.\end{cases}$$

The radiation term $Q_r$ in (5) is calculated using the data in [7], when $T>10\,200$ K; and when $9500\ \text{K}<T<10\,200$ K, the following is used:

$$Q_r=5.6\times10^{-3}(T-9500)\cdot0.18\times10^{-3}(T-9500)^2\ \text{W/cm}^3$$

and

$$\xi=4\pi\times10^{-9}\ \text{H/cm}$$
$$\omega=2\pi\times4\times10^6/\text{s}.$$

The boundary conditions of (1)–(6) are as follows.

1) Inlet conditions ($x=0$):

$$0\le r\le R_i,\quad u=Q_{\text{Ari}}/\pi R_i^2$$
$$v=0$$
$$C_{\text{Ar}}=1.0$$
$$w=Q_{Ari}(r/R_i)/(\pi R_{\text{in}}^2)$$
$$T=350\ \text{K}$$
$$R_i<r\le R_0,\quad u=(Q_{\text{Aro}}+Q_{\text{SiCl}_4})/\{\pi[(R_0^4-R_i^4)-(R_0^2-R_i^2)/\ln(R_0/R_i)]\}\times[R_0^2-r^2+(R_0^2-R_i^2)\cdot\ln(r/R_0)/\ln(R_0/R_i)],$$
$$C_{\text{Ar}}=M_{\text{Ar}}Q_{\text{Ar}}/(M_{\text{Ar}}Q_{\text{Ar}}+M_{\text{SiCl}_4}Q_{\text{SiCl}_4})$$
$$C_{\text{SiCl}_4}=M_{\text{SiCl}_4}Q_{\text{SiCl}_4}/(M_{\text{Ar}}Q_{\text{Ar}}+M_{\text{SiCl}_4}Q_{\text{SiCl}_4})$$
$$T=350\ \text{K}. \quad (12)$$

2) Centerline ($r=0$):

$$v=w=0$$
$$\partial\phi/\partial T=0,\quad \phi=u,\ C_i,\ T. \quad (13)$$

3) Condition on the inner wall in the reactor and side inlet:

$$u=v=w=0$$
$$\partial C_i/\partial n=0. \quad (14)$$

4) Sidewall inlet condition ($L_3\le x\le L_3+h$, $r=R_{\text{sto}}$):

$$u=w=0$$
$$v=-(Q_{\text{H}_2}+Q_{\text{NH}_3})/(2\pi R_{\text{sto}}h)$$
$$C_{\text{H}_2}=M_{\text{H}_2}Q_{\text{H}_2}/(M_{\text{H}_2}Q_{\text{H}_2}+M_{\text{NH}_3}Q_{\text{NH}_3})$$
$$C_{\text{NH}_3}=M_{\text{NH}_3}Q_{\text{NH}_3}/(M_{\text{H}_2}Q_{\text{H}_2}+M_{\text{NH}_3}Q_{\text{NH}_3}). \quad (15)$$

5) Exit ($x=LT$):

$$\partial\phi/\partial x=0,\quad \phi=u,\ C_i$$
$$\partial^2v/\partial x^2=\partial^2w/\partial x^2=0. \quad (16)$$

6) The temperature at the outer wall of the reactor is

$$T=350\ \text{K}.$$

The temperature of the water-cooling tank is

$$T=323\ \text{K}. \quad (17)$$

The boundary conditions for the electromagnetic field equations (8)–(10) are set at $r=0$ and $0\le x\le L_3$, which are

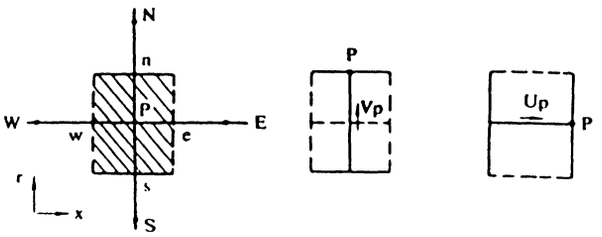


(a) (b)

Fig. 3. Control volume in SIMPLER: (a) for a general dependent variable ($p$, $w$, $T$, $C_i$); (b) for the velocity components $u$ and $v$.

TABLE I
DEPENDENT VARIABLE $\phi$, DIFFUSION COEFFICIENT $\Gamma_\phi$, AND SOURCE TERM $S_\phi$

| Eq | $\phi$ | $\Gamma_\phi$ | $S_\phi$ |
|---|---|---|---|
| Continuity | 1 | 0 | 0 |
| x Momentum | u | $\mu$ | $\frac{\partial}{\partial x}(\mu\frac{\partial u}{\partial x}) + \frac{1}{r}[\frac{\partial}{\partial r}(\mu r\frac{\partial v}{\partial x})] + \rho g - \frac{\partial p}{\partial x}$ |
| r Momentum | v | $\mu$ | $\frac{\partial}{\partial x}(\mu\frac{\partial u}{\partial r}) + \frac{1}{r}[\frac{\partial}{\partial r}(\mu r\frac{\partial v}{\partial r})] - \frac{2\mu v}{r} + F_r - \frac{\partial p}{\partial r} + \frac{\rho w^2}{r}$ |
| $\theta$ Momentum | w | $\mu$ | $-W[\frac{\rho v}{r} + \frac{1}{r}(\frac{\partial \mu}{\partial r}) + \frac{\mu}{r^2}]$ |
| Diffusion | $C_i$ | $\rho D_i$ $(=\mu)$ | 0 |
| Energy | T | $k/\bar{c}_p$ | $(P-Q_r) - \{\frac{k}{r}[\frac{\partial}{\partial x}(\frac{r}{\bar{c}_p}\frac{\partial T}{\partial x})]\}$ *) |
| *) Negelet | | | $\Sigma C_{pi}(\rho D_i\frac{\partial C_i}{\partial x})\frac{\partial T}{\partial x} + \Sigma C_{pi}(\rho D_i\frac{\partial C_i}{\partial r})\frac{\partial T}{\partial r}$ |

$$x = \pi/2, \qquad dx/dr = 0$$
$$E_\theta = 0, \qquad dE_\theta/dr = -\xi\omega H_x/2$$
$$H_x = H_c, \qquad dH_x/dr = 0. \tag{18}$$

Here

$$H_C = [NI/2(L^2 - L_1)][(L_2 - x)/\sqrt{R_{Ci}^2 + (L_2 - x)^2} - (L_1 - x)/\sqrt{R_{Ci}^2 + (L_1 - x)^2}].$$

The electric current $I$ is not specified; rather, the total power input to the plasma $P_0$ is known. This is set as an integral-type boundary condition

$$P_t = \int_0^{L3}\int_0^{R0} 2\pi rp dr dx \tag{19}$$

and if $P_t \neq P_0$, a correction factor to the electric and magnetic fields is found: $\alpha_c = \sqrt{P_0/P_t}$, multiplying the electromagnetic fields by $\alpha_c$ ensures the condition $P_t = P_0$ to be satisfied.

## III. Numerical Procedure

The electromagnetic field equations (8)–(10) are solved using a fourth-order Runge–Kutta method. Equations (1)–(6) are solved by using a SIMPLER algorithm [8], which is a general algorithm for the solution of elliptic fluid flow, heat transfer, and diffusion problems, and is based on a scheme developed by Patankar and Spalding. The scheme is formulated to solve the conservation laws written in the following general form:

$$\frac{\partial}{\partial t}(\rho\phi) + \nabla(\rho\phi\bar{V}) = \nabla(\Gamma_\phi\nabla\phi) + S_\phi \tag{20}$$

where $\phi$ is called the dependent variable, $\Gamma_\phi$ and $S_\phi$ are the diffusion coefficient and the source term, respectively. Table I shows the dependent variables, the diffusion coefficients, and the source terms for (1)–(6). A general numerical scheme is obtained by integrating (20) over a control volume

$$(a_p - S_p)\phi_p = \sum_{i=E,W,N,S} a_i\phi_i + b_p \tag{21}$$

where $a_i$ includes the contribution of the convection and diffusion terms; $S_p$ and $b_p$ are the coefficient of linear term and constant term in (21), respectively; $a_i$ is derived using a power-law scheme. The meanings of the subscripts $P$, $E$, $W$, $N$, and $S$ are shown in Fig. 3. Applying (20) to (2)–(6), we get the discretized equations for $u$, $v$, $C_i$, $T$, $w$, and the control volumes for $u$ and $v$ are staggered (Fig. 3). From the discretized equations of $u$, $v$, and the continuity equation, the discretized equations for pressure and for pressure correction are obtained.

The shape of the flow path in the equipment is very complicated, and our meshes and control volumes cover the whole flow field of the torch, the reactor, the water-cooling tank, and their walls, and it is very dense: 90 × 35. In order to make wall velocity zero, the viscosity here is set to be a large number (a million times that of gases), and the velocity boundary condition on the outer wall surface assumes zero. Moreover, $S_p$ here also equals a large

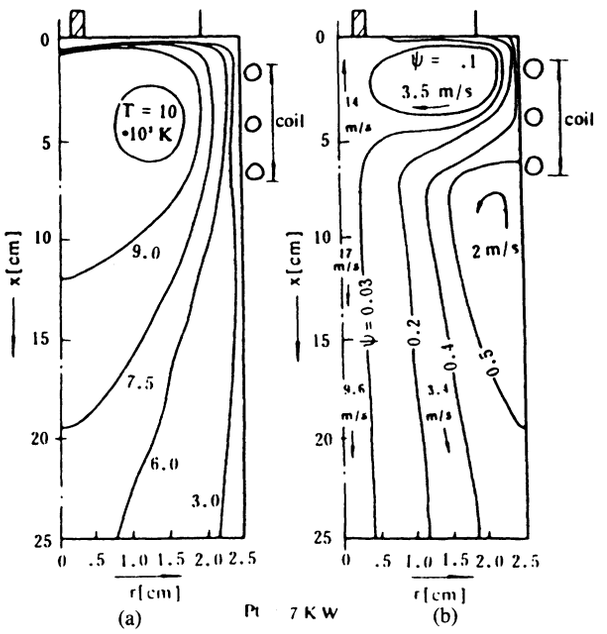


Fig. 4. (a) and (b) The numerical check for a plasma torch.

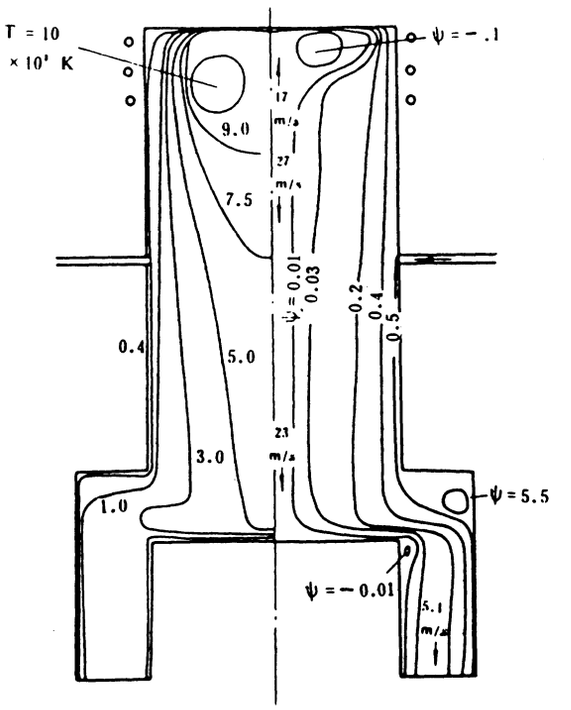


Fig. 5. Isotherm contours and streamlines in the CVD reactor with heating and without swirling.

number ($10^{30}$) and $b_p = 0$; the diffusion coefficient here is assumed to be zero and $C_i$ on the wall outer surface is assumed to be zero, too. This is a way to give a boundary condition, which is different from the ordinary method. For instance, we always make equal the values at two neighboring mesh points to ensure $\partial C_i/\partial n = 0$. The line which joins the points is perpendicular to the wall. The exit condition of the flow field is the key for the convergence of the calculation. The method we used is to modify velocity $u$ and the concentrations here and to make the mass and species satisfy the conservation condition in whole flow fields. Practice proves that this is an effective method. The relaxation factors vary between 0.3 and 0.8 during iteration.

To justify the convergence of our computation, a maximum residue for each dependent variable is defined at each iteration. For the $n$th iteration it is defined as

$$R_n(\phi) = \text{Max } |\phi_{ij}^n - \phi_{ij}^{n-1}|/\text{Max } |\phi_{ij}^n|. \qquad (22)$$

A converged solution is obtained when $R_n(\phi)$, for all the dependent variables, is less then 0.3 percent.

In order to check the validity of our mathematical model and our numerical procedure and algorithm, we calculated the field of a torch with the same operating conditions and geometric structure of Mostaghimi *et al.* [9]. Although the assumed boundary conditions and the physical properties of Ar are slightly different from theirs, the isotherm contours and streamlines are almost the same (see Fig. 4) except for the velocities indicated in the figure. We further checked the difference by an obvious but approximate relation $(\bar{u}r^2/\bar{T}\psi)_{\text{exit}} = 2/\pi x(Q/T\rho)_{\text{inlet}}$, where $\bar{u} = \int_0^r ur\,dr/\frac{1}{2}r^2$ and the same for $\bar{T}$, and concluded that there exists no contradiction in our results.

## IV. Results and Discussion

Calculation is made under atmospheric pressure at a power level of 8.4 kW with argon as a heating gas and

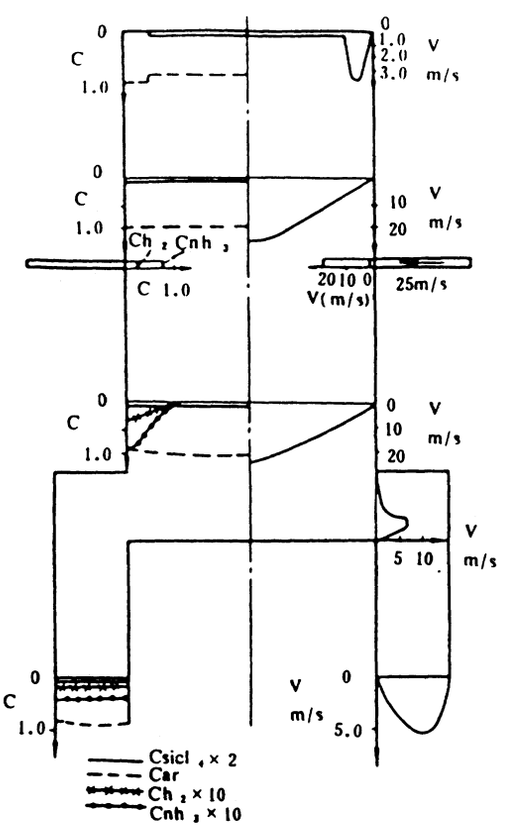


Fig. 6. Velocity and concentration distributions in some typical positions in the CVD reactor with heating and without swirling.

$SiCl_4$, $NH_3$, and $H_2$ as reactants. The operating conditions of the plasma CVD reactor are shown in Fig. 2. The results obtained are as follows.

Fig. 5 shows the streamlines and the isotherm contours without swirling. Fig. 6 shows the velocity and concen-

tration profiles in several typical positions in the flow field under the same conditions. Obviously the flow field is very complicated. There exist four eddy rings and a flow around a blunt body. The magnetoelectric pumping at the center of the coil induces a strong inward radial flow (4.5 m/s) with the formation of a recirculation eddy ring, which causes a back flow on the order of 17 m/s. The flow downstream of this first eddy appears parabolic. The second eddy ring, which is not shown in the figure for its smallness, is situated at the immediate downstream of the side injection slit and near the wall. It can just be judged from the computational data. The third one is at the corner formed in the conjunction place between the graphite tube and the collection tube, while the fourth one is situated at the shoulder of the water-cooling tank. The flow around the cooling tank is something like a parallel flow around a blunt body.

The electromagnetic heating induces an interesting dent in the temperature contours around the middle of the induction coil as shown in Fig. 5. This effect is simply caused by the pumping of cold gas from the outer region near the wall into the fireball and was first pointed out by Boulos [3]. The highest temperature in the field is about 10 200 K, and the temperature at the center of the reaction chamber is about 3000–6000 K. The temperature is about 1000–3000 K in the region where the mixing between $H_2$, $NH_3$, Ar, and $SiCl_4$ is very dramatic. After the flow meets the water-cooling tank, the gas temperature decreases to 1000–2500 K. Considering that the favorable temperature for $3SiCl_4 + 4NH_3 + nH_2 = Si_3N_4 + 12HCl + nH_2$ is about 1750 K [1], the reaction is an endothermic one, and the core flow of the reaction chamber is still in high temperature. We can conclude that the equipment studied is reasonable for the formation of $Si_3N_4$ vapor. The temperature at the water-cooling tank is very low and the fluid particles near it must spend more time flowing downstream, so that it is beneficial to the crystallization of the vapor.

Although the third and fourth eddy rings can enhance mixing between species, their existence may make $Si_3N_4$ crystal hit the walls of the collection tube and water-cooling tank and adhere to them. This is a harmful effect to our chemical process, and the configuration of the reactor must be improved. How to use numerical simulation to help us improve the configuration of the equipment will be presented elsewhere.

We also have studied the effect of the change of side injection slit width and the swirl on the flow field [10]. We do not want to describe the details of these effects because of the limited space. Briefly, the narrowing of the slit may enhance the mixing of species, but just slightly affects the contours of the streamlines and isotherms. As an example, Fig. 7 shows that when $h$ changes from 0.1 mm (right) to 0.01 mm (left), the higher concentration region of $NH_3$ becomes smaller, while the lower concentration region becomes larger. Similar changes also take place for the concentration of $SiCl_4$, $H_2$, and Ar. Swirling of the flow at the inlet may cause the movement and size

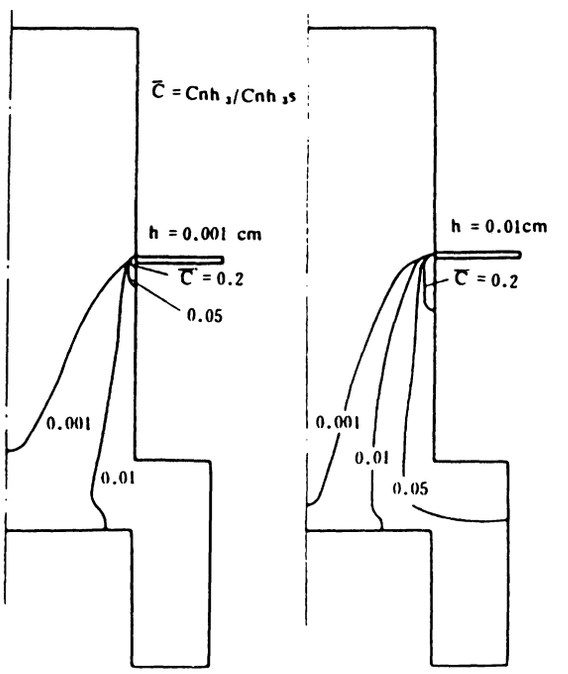


Fig. 7. The effect of side injection slit width on species diffusion in the CVD reactor with heating and without swirling.

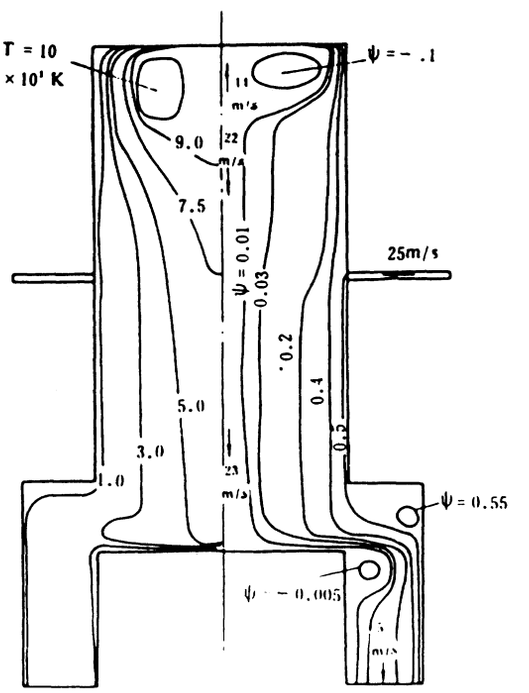


Fig. 8. Isotherm contours and streamlines in the CVD reactor with heating and swirling (see Fig. 9 for swirling velocity).

change of the eddies, as can be seen in Figs. 8 and 9, and slightly affects the distribution of the other velocity components. Fig. 9 also shows the decreasing process of swirling. These are two very important phenomena which can be used by design engineers both in the research lab and in industry. For example, the magnitude of $h$ can be adjusted so that the mixing of $SiCl_4$, $NH_3$, and $H_2$ is taking place at the region where the temperature is the most favorable—one for the required chemical reaction.

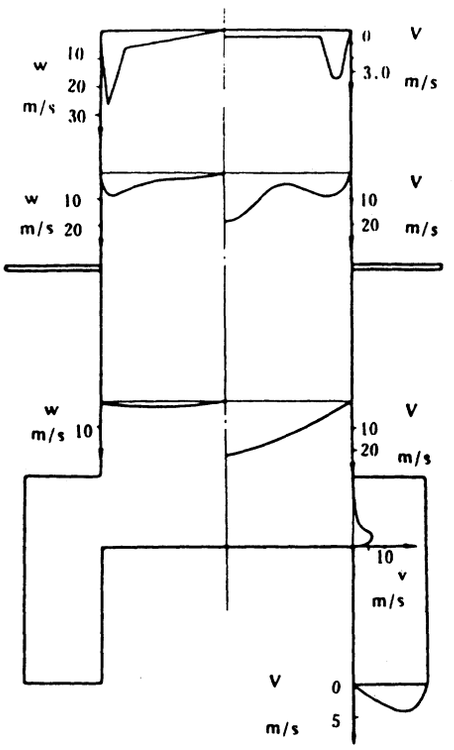


Fig. 9. Swirl velocity $w$ distribution and its effect on $u$ and $v$ components with heating.

## V. Conclusions

This paper formulates a mathematical model for the numerical simulation of the flow field in a plasma CVD reactor. Using the algorithm of Patankar and Spalding, we have calculated the flow, temperature, and concentration fields without taking the chemical reaction and crystallization into account. From the obtained results we get the following conclusions.

1) Although we use temperature (not enthalpy) as the dependent variable and some slightly different boundary conditions, we get the same flow field in an RF plasma torch as Boulos gets.

2) The flow fields in the RF plasma CVD reactor is very complicated, and it includes four recirculation regions and a flow around a blunt body. Computation reveals that the design of the plasma CVD reactor is reasonable from an overall consideration, but there are two recirculation regions which can cause the particles formed during crystallization to adhere to the wall of the reactor and are harmful to the working process. Improvement of the structure is necessary.

3) The side injection slit width and swirl of the flow have some obvious effects on the concentration and the flow fields, respectively. These are two important phenomena which deserve more detailed research and can be used by designers.

4) Owing to the lack of the related chemical reaction rate, we cannot take the chemical reaction and crystallization into consideration, thus more study is needed. In spite of that, we have still obtained a lot of very useful insight into the phenomenon that exists in the plasma CVD reactor.

## Acknowledgment

The authors wish to thank Prof. Chen Xi for his helpful discussion with us.

## References

[1] Z. Ching-Wen and Y. Jie-Peng, presented at the 7th Int. Symp. Plasma Chem., Eindhoven, Netherlands, Paper B-4-1, July 1985.
[2] Z. Guo-Ying and Z. Ching-Wen, in *Proc. 3rd Chinese Nat. Cong. Computational Fluid Mech.* (Chang Sai, China), Nov. 1985.
[3] M. I. Boulos, *IEEE Trans. Plasma Sci.*, vol. PS-4, pp. 28-39, 1976.
[4] M. I. Boulos and Ronald Gagne, CJChE, vol. 58, pp. 367-375, 1980.
[5] T. Yoshida, K. Nakagawa, T. Harada, and K. Akashi, *Plasma Chem. Plasma Processing*, vol. 1, 1981, pp. 113-128.
[6] T. Harada, T. Yoshida, T. Koseki, and K. Akashi, *J. Japan Inst. Metals*, vol. 45, no. 11, pp. 1138-1145, 1981.
[7] D. L. Evans and R. S. Tankin, *Phys. Fluids*, vol. 10, pp. 1137-1144, 1967.
[8] S. V. Patankar, *Numerical Heat Transfer and Fluid Flow.* New York: McGraw-Hill, 1980.
[9] J. Mostaghimi, P. Proulx, and M. I. Boulos, *Numerical Heat Transfer*, vol. 8, pp. 188-201, 1985.
[10] Z. Guo-Ying and Z. Ching-Wen, in *Proc. 3rd Chinese Nat. Cong. Computational Fluid Mech.* (HangChou, China), June 1986.
[11] Z. Ching-Wen, *Advances in Mechanics*, vol. 16, no. 2, 1986.